Speciation driven by ancestrally polymorphic chromosomal inversions

Running title: Inversions and speciation in *Drosophila*

Authors:

Poikela, N.[1], Laetsch, D. R.[2], Lohse, K.[2*], & Kankare, M[1*].

[1] Department of Biological and Environmental Science, University of Jyväskylä, Finland

[2] Institute of Evolutionary Biology, University of Edinburgh, United Kingdom

[*] these authors contributed equally

Corresponding author:

Noora Poikela, Department of Biological and Environmental Science, P.O. Box 35, FI-40014, University of Jyväskylä, Finland

e-mail: noora.p.poikela@gmail.com

Abstract

Chromosomal inversions may play a central role in speciation given their ability to reduce recombination and therefore genetic exchange at parts of the genome between diverging populations. We analysed long- and short-read whole-genome data from sympatric and allopatric populations of two *Drosophila virilis* group species, *D. montana* and *D. flavomontana*, to understand how inversions have contributed to their divergence. We identified three large alternatively fixed inversions on the X chromosome and one on each of the autosomes 4 and 5. A comparison of demographic models estimated for inverted and non-inverted (colinear) chromosomal regions suggest that these inversions arose before the time of the species split. We detected low rate of interspecific gene flow (introgression) from *D. montana* to *D. flavomontana*, which was further reduced inside inversions and was lower in allopatric than in sympatric populations. Together, these results suggest that the inversions were already present in the common ancestral population, and that gene exchange between the sister taxa was reduced within inversions both before and after the onset of species divergence. Such ancestrally polymorphic inversions may act as drivers of speciation by allowing the accumulation of genetic divergence and incompatibilities inside inversions, while gene exchange at colinear regions continues until the evolving reproductive barriers complete speciation. The overlapping X inversions are particularly good candidates for driving the speciation process of *D. montana* and *D. flavomontana*, since the strongest genetic incompatibilities detected in a study of experimental introgression reside within these inversions and prevent introgression between the species.

Key words: chromosomal inversion, coalescence, *Drosophila*, genetic divergence, introgression, speciation

Introduction

Understanding the speciation process and its genetic basis remains a major goal of evolutionary biology. Chromosomal inversions, genomic regions with reversed gene order, may facilitate adaptation and speciation in the face of gene flow because they suppress recombination between alternate rearrangements, which creates and preserves associations between sets of alleles conferring local adaptation, mate choice and genetic incompatibilities (Sturtevant 1921; Butlin 2005; Hoffmann and Rieseberg 2008). While inversions have been found in many species of insects, fish, birds, mammals and plants, their frequency varies widely between and even within taxa (Stone et al. 1960; Wellenreuther and Bernatchez 2018) and it remains an open question whether and how inversions contribute to the evolution of species divergence. Genomic data from young species pairs, together with quantitative inference of the history of inversions and interspecific gene flow (introgression), offers a promising way to investigate the role of inversions in speciation (Faria and Navarro 2010; Faria et al. 2018).

Inversions may facilitate adaptation and speciation in many ways (reviewed in Hoffmann and Rieseberg 2008; Jackson 2011; Faria et al. 2018). A new inversion may be favoured by selection if it protects locally adapted allele combinations from recombination with maladapted immigrant alleles that reside in an alternate rearrangement (Kirkpatrick and Barton 2006). Also, inversion breakpoints may be direct targets of selection, if they change the reading frame and/or expression patterns of genes located at the breakpoint (Matzkin et al. 2005; Guerrero et al. 2012). While under the model of Kirkpatrick and Barton (2006) the probability of fixation of an inversion linking locally adaptive alleles between divergent populations depends on gene flow, its potential to contribute to the speciation process in the long term also depends on whether the populations evolve in isolation or in the face of gene flow. Allopatry inevitably leads to a build-up of genetic incompatibilities as an incidental by-product of drift and selection throughout the whole genome (Seehausen et al. 2014). Upon secondary contact, genetic incompatibilities residing within inversions will be protected, while those located at non-inverted (colinear) regions are more susceptible to the homogenizing effects of gene flow (Noor et al. 2001). In contrast, for populations that diverge in the presence gene flow, the accumulation of genetic divergence and genetic incompatibilities may be (at least initially) restricted to inverted regions (Navarro and Barton 2003). In both scenarios, inversions harbouring incompatibilities delay species' fusion and provide time for additional barriers to evolve. For example, prezygotic reproductive barriers are expected to be more easily reinforced in response to genetic incompatibilities and maladaptive hybridization (reinforcement) (Servedio and Noor 2003), if the causal loci are located within inversions (Trickett and Butlin 1994; Butlin 2005; Dagilis and Kirkpatrick 2016). Two kinds of empirical observations give indirect support for these theories. First, genes maintaining local adaptation, premating barriers and genetic incompatibilities between species have been found to be concentrated in alternatively fixed inversions (Noor et al. 2001;

Lowry and Willis 2010; Fishman et al. 2013). Second, fixed inversions generally have elevated genetic divergence compared to colinear regions (Noor et al. 2007; Kulathinal et al. 2009; Lohse et al. 2015). However, it has proven difficult to distinguish speciation histories in which inversions have acted as triggers of speciation from scenarios in which the alternately fixed inversions arise incidentally (Faria and Navarro 2010; Guerrero and Hahn 2017; Fuller et al. 2019).

So far only a few studies have dissected the evolutionary history of inversions to explore their role in adaptation (Lundberg et al. 2023) and speciation (e.g. Lohse et al. 2015; Fuller et al. 2018). Demographic models can be used to systematically compare the species' divergence and the amount of long-term effective introgression (*M*) between inverted and colinear regions (Noor and Bennett 2009). Similarly, recent or ongoing introgression can be diagnosed by comparing estimates of *M* between sympatric and allopatric population pairs (Noor and Bennett 2009). There are at least three scenarios for the evolutionary history of alternately fixed inversions. First, inversions, which have arisen and fixed after the speciation is largely complete, most likely became established for reasons that have little to do with speciation. In this case, we expect reduced introgression ($M_{inv} < M_{col}$) within inversions, but the same split time estimates for inversions and colinear regions ($T_{inv} = T_{col}$). Second, inversions may become fixed during the speciation process because they have acted as barriers for gene flow at an early stage of high gene flow (Kirkpatrick and Barton 2006). Such inversion should have reduced introgression compared to colinear regions ($M_{inv} < M_{col}$) and their estimated divergence time either predates that of colinear regions ($T_{inv} > T_{col}$) (if they have been segregating in the common ancestral population) or is the same ($T_{inv} = T_{col}$) (if they arose at the onset of divergence). Crucially however, irrespective of their age, we expect that inversions that have fixed because they protect co-adapted alleles from disassociation in the face of gene flow to harbour strong barrier loci (e.g. BDMIs). Finally, in a third scenario, inversions are segregating in the ancestral population due to forces that have nothing to do with local adaptation or species divergence, e.g. balancing selection. In this case, we would expect inversions to be alternately fixed in the two species by chance alone with the probability of 0.5 (Guerrero and Hahn 2017). In other words, the predictions for this scenario in terms of demographic parameters are the same as in the second scenario above. Importantly, however, we would not expect an enrichment of inversions for barrier loci.

The two *Drosophila virilis* group species, *Drosophila montana* and *Drosophila flavomontana*, offer a great opportunity to investigate the potential role of inversions in speciation. Based on polytene chromosome studies, these species have several alternatively fixed inversions (Stone et al. 1960; Throckmorton 1982), which, however, have so far not been characterised at the genomic level. *D. montana* and *D. flavomontana* have diverged ~3.8 Mya in the Rocky Mountains, and the two species presently inhabit variable climates in the Rocky Mountains and along the western coast of North

America (Hoikkala and Poikela 2022; Yusuf et al. 2022). In the mountains, *D. montana* has spread to higher altitudes than *D. flavomontana*, while on the western coast, where *D. flavomontana* has expanded relatively recently, both species live at low altitudes (Fig. 1, Table S1; Patterson 1952; Hoikkala and Poikela 2022). Thus, in both regions, populations of the two species can be regarded as sympatric or parapatric. However, *D. montana* also has allopatric populations at high latitudes, e.g. in Alaska, where *D. flavomontana* does not exist (Fig. 1, Table S1). *D. montana* and *D. flavomontana* are separated by strong pre- and postzygotic barriers across their range, and *D. flavomontana* also show signs of reinforcement in prezygotic barriers in sympatric populations (Poikela et al. 2019). Despite this strong reproductive isolation, interspecific hybrids have been found in nature (Patterson 1952; Throckmorton 1982) and can also be produced in the laboratory (Poikela et al. 2019). Importantly, evidence for strong BDMI(s) between these species located within inversions on the X chromosome has been found (Poikela et al. 2022). This prevents introgression from *D. montana* to *D. flavomontana* across the entire X chromosome during early backcross generations (Poikela et al. 2022).

Here, we explored whether and how inversions have contributed to the species divergence of *D. montana* and *D. flavomontana*. We used long- and short-read sequencing data from allopatric and sympatric populations of the species to generate highly contiguous assemblies for both species, which in turn enabled us to accurately identify the presence of alternatively fixed inversions. We used demographic modelling to estimate the age of these inversions and their potential effect on the long-term rate of introgression and asked the following specific questions:

(1) How many alternatively fixed inversions do *D. montana* and *D. flavomontana* carry?

(2) When did these inversions most likely arise and how does their age compare to the species divergence time?

(3) Do these inversions show elevated divergence and reduced introgression compared to colinear regions, indicating their ability to suppress recombination and introgression?

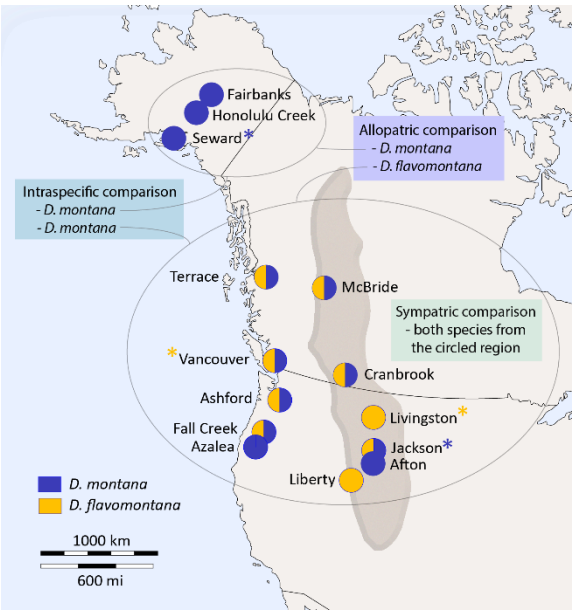

Figure 1. Sampling sites of sympatric (or parapatric) and allopatric *D. montana* and *D. flavomontana* populations in North America. Pie charts indicate the sampling sites for one or both species. Long-read PacBio data were obtained from two isofemale strains per species (sample sites indicated with asterisks). Short-read Illumina data were obtained from single wild-caught females for all sites shown.

Results and Discussion

We generated long-read PacBio (Pacific Biosciences) sequencing data for females from two *D. montana* and two *D. flavomontana* isofemale strains and short-read Illumina re-sequencing data for 12 *D. montana* and 9 *D. flavomontana* wild-caught females (one female per population per species) originating from allopatric and sympatric populations (Fig. 1, Table S1). These data enabled us to generate contiguous, high-quality genome assemblies for both species to accurately identify alternatively fixed inversions and to examine the species' evolutionary history and the role of inversions and introgression therein. In the following, we refer to comparison between *D. montana* and *D. flavomontana* samples from the Rocky Mountains and the western coast as "sympatric", and the comparisons between *D. montana* from Alaska and *D. flavomontana* from the mountains and the coast as "allopatric" (Fig. 1, Table S1). To evaluate the timing of potential recent introgression in sympatry, we estimated the divergence time for *D. montana* living in contact (sympatry) and in isolation (allopatry) with *D. flavomontana*, and we refer to this comparison as "intraspecific" (Fig. 1, Table S1).

Construction and annotation of species genomes

Two genome assemblies for each species were generated using the PacBio data of two *D. montana* and *D. flavomontana* isofemale strains and the Illumina data for the respective founder females collected from the wild (Table S1, S2). The assembled genomes had a total length of 181-194Mb (Table 1), which

149 resemble those of previously assembled *D. montana*, *D. flavomontana* and several other *Drosophila*
150 species (128-198Mb) (Miller et al. 2018; Parker et al. 2018; Yusuf et al. 2022). A small proportion of each
151 assembly (0-18 contigs, spanning = 0.0-9.9Mb) was excluded as contaminant sequences, mainly
152 bacteria, based on the coverage, GC% and taxonomic annotation of contigs (Fig. S1-S4). From the 3285
153 BUSCO groups, we identified 97.3-98.5% as complete BUSCOs, of which 96.9-98.0% were single-copy
154 and 0.4-0.5% duplicated BUSCOs (Table 1). The BUSCO values were similar to the ones in other
155 *Drosophila* assemblies (Miller et al. 2018). Repetitive sequences comprised 25.5-29.9% of our
156 assemblies (Table 1), which is close to the repeat content reported for other *Drosophila* species (e.g.
157 26.5% in *D. virilis*, 28.6% in *D. melanogaster*, 22.9% in *D. mojavensis*, and 19.9% in *D. elegans*; NCBI
158 Annotation Report). Our annotations included 15,696-16,047 genes per assembly, which is plausible
159 given the number of genes reported for other *Drosophila* assemblies (e.g. Yang et al. 2018). Overall, the
160 combination of long- and short-read data resulted in more contiguous assemblies for both species (N50
161 values of 1.3-11.0Mb; Table 1) compared to the previously published *D. montana* and *D. flavomontana*
162 genomes which were based on short-read data (e.g. N50 of 41kb in *D. montana;* Parker et al. 2018;
163 Yusuf et al. 2022).

164 We built a chromosome-level reference genome for *D. montana* by scaffolding with the *Drosophila*
165 *lummei* genome, and for *D. flavomontana* by first scaffolding one assembly with the other (within
166 species) and then with the *D. lummei* genome (see Methods for details). For both chromosome-level
167 genomes, the total genome size, BUSCO values and the number of repeats and genes slightly decreased
168 compared to the original, non-scaffolded assemblies (Table 1). Given greater span and completeness
169 (as measured by BUSCO) of the *D. montana* compared to the *D. flavomontana* genome, subsequent
170 analyses were performed using the *D. montana* as a reference by default. However, to quantify the
171 effect of reference bias, we repeated the demographic inference using *D. flavomontana* as a reference.

172 Table 1. Contiguity, completeness, and annotation of original and scaffolded chromosome-level genome
173 assemblies.

		D. montana Seward, USA monSE13F37	*D. montana* Jackson, USA monJX13F48	*D. flavomontana* Livingston, USA flaMT13F11	*D. flavomontana* Vancouver, Canada flaVAN14F20	*D. montana* chromosome-level reference genome	*D. flavomontana* chromosome-level reference genome
Genome contiguity							
	Genome size (Mb)	184.3	181.0	192.6	193.5	145.5	142.3
	Total contigs	324	796	376	296	6	6
	Longest contig (Mb)	29.1	15.2	29.0	26.8	32.5	30.7
	N50 (Mb)	11.0	1.3	9.8	7.8	26.5	27.2
	N50 count	5	20	6	6	3	3
Genome completeness							
	Total complete BUSCOs (%; n: 3285)	98.1	98.5	97.5	97.3	91.9	91.5
	Single copy BUSCOs (%)	97.6	98.0	97.1	96.9	91.7	91.2
	Duplicated BUSCOs (%)	0.5	0.5	0.4	0.4	0.2	0.3
Genome annotation							
Repeat elements	**GC level (%)**	40.2	40.2	40.2	40.1	40.3	40.3
	Masked repeats (%)	26.6	25.5	29.9	28.2	16.8	15.1
Gene annotation	**Genes (N)**	15,696	15,819	15,940	16,047	15,446	14,901
	Mean gene length (bp)	1,640	1,637	1,568	1,564	1,571	1,557
	Total complete BUSCOs (%; n: 3285)	94.2	94.7	92.5	92.9	88.5	87.3
	Single copy BUSCOs (%)	84.4	84.5	84.1	84.5	79.9	79.3
	Duplicated BUSCOs (%)	9.8	10.2	8.4	8.4	8.8	8.0

174

175 N50 = half of the genome is in contigs larger than or equal to the N50 contig size. N50 count = half of the genome
176 consists of the number indicated in N50 count.

177 Genetic differentiation and climatic variability of *D. montana* and *D. flavomontana* populations

178 To investigate the genetic structure of *D. montana* and *D. flavomontana* populations, we performed a
179 principal component analysis (PCA) on the Illumina re-sequence data for the 12 and 9 wild-caught
180 females of *D. montana* and *D. flavomontana*, respectively (Table S1 & S2). The PCA included 9,064,171
181 filtered SNPs from coding, intronic and intergenic regions. The first two principal components (PCs) had
182 Eigenvalues >1, and PC1 explained majority (50%) of the total genetic variance and clearly separated *D.*
183 *montana* and *D. flavomontana* samples from each other (Fig. 2A, Table S3). PC2 explained 4% of the
184 total variance and captured variation mainly within *D. montana*, while variation in *D. flavomontana* was
185 lower (Fig. 2A, Table S3). PC2 separated Alaskan/allopatric *D. montana* populations (Honolulu Creek,
186 Seward, Fairbanks) from *D. montana* populations in the Rocky Mountains and the western coast, but
187 also showed some variation among these two groups (Fig. 2A, Table S3).

188 Next, we explored climatic variability of fly sampling sites to determine the extent to which climatic
189 conditions may have affected the genetic differentiation of the samples. We performed a PCA on 19
190 bioclimatic variables of each fly sampling site (Table S4, S5) to reduce correlations between the variables
191 and summarized climatic patterns prevailing in the sites. This PCA revealed three principal components
192 (PCs) with Eigenvalues >1, of which the first two PCs explained ~80% of the climatic variation (Fig. 2B,
193 Table S6). The first PC clearly separated inland and coastal populations and suggested that populations
194 from the mountainous inland experience cold winters and high seasonal temperature variation, while
195 coastal populations experience milder temperatures and high precipitation throughout the year (Fig.
196 2B, Table S7). The second PC separated populations based on summer temperatures and variation in

diurnal temperatures and distinguished Alaskan populations (Honolulu Creek, Seward, Fairbanks) from the other populations (Fig. 2B, Table S7).

Together these results show that *D. montana* and *D. flavomontana* populations are genetically diverged regardless of their climatic origin and species coexistence. Genetic differentiation was greater among *D. montana* populations than among *D. flavomontana* populations, which is likely due to *D. montana*'s larger geographic range and the fact that *D. flavomontana* has spread across North America more recently than *D. montana* (Hoikkala and Poikela 2022). Finally, the genetic differentiation between allopatric (from Alaska) and sympatric (from the Rocky Mountains and the western coast) *D. montana* populations likely reflects a demographic history of intraspecific divergence, local adaptation to climatic conditions, or both.

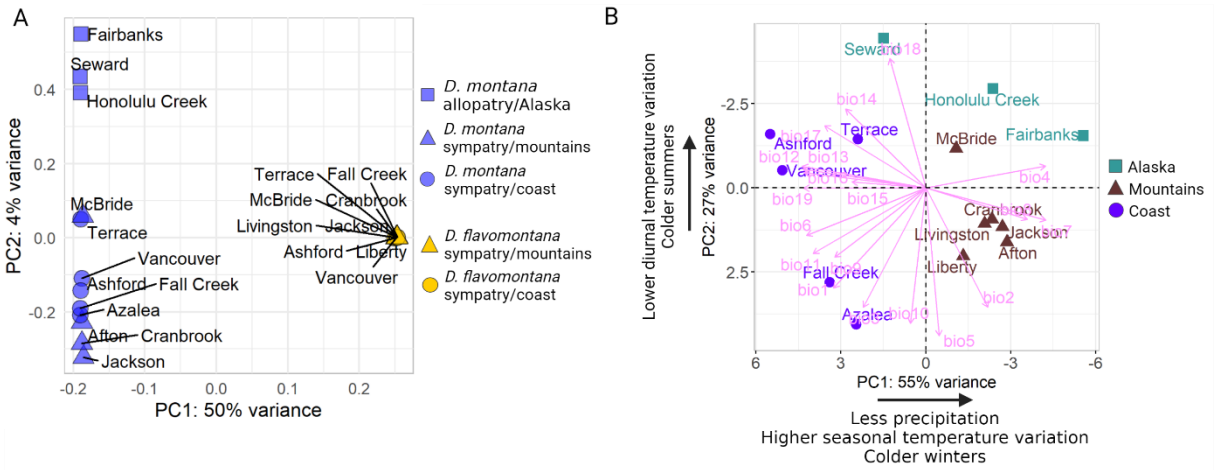

Figure 2. A principal component analysis (PCA) (A) on whole-genome SNP data of *D. montana* and *D. flavomontana* samples originating from different sites of North America and (B) on 19 bioclimatic variables (detailed explanations in Table S4) of each fly sampling site.

D. montana and *D. flavomontana* chromosomes differ by several large inversions

We combined long- and short-read genomic data to characterize inversion breakpoints in *D. montana* and *D. flavomontana*. We identified five large (>0.5Mb) inversions that were alternatively fixed between North American *D. montana* and *D. flavomontana* samples (Fig. 3, Table S8). The X chromosome contained three partly overlapping inversions, two of which were fixed in *D. montana* (7.2Mb and 14.2Mb) and one in *D. flavomontana* (3.2Mb) (Fig. 3, Table S8). Chromosomes 4 and 5 each contained one inversion fixed in *D. flavomontana* (13.8Mb and 9.2Mb, respectively) (Fig. 3, Table S8). All these inversions were homozygous in Illumina re-sequence individuals of both species (Table S8). In contrast, chromosomes 2 and 3 did not contain any fixed inversion differences, but the left arm of the 2nd chromosome (2L) contained one heterozygous *D. montana* inversion (3.9Mb) (Fig. 3, Table S8) which

221 was excluded from further analysis altogether. The sizes of inversions were obtained from the genome
222 assemblies of each species (Table S8).

223 Based on polytene chromosome studies (Stone et al. 1960), the three alternatively fixed inversions
224 between *D. montana* and *D. flavomontana* on the X chromosome likely correspond to inversions E, F
225 and G. These inversions were not distinguished in more detail in Stone et al. (1960), and, in contrast to
226 our results, Stone et al. (1960) suggest that all three X inversions are fixed in *D. flavomontana*. The
227 inversions on the 4th and 5th chromosome have been named J and E in karyotype studies, respectively
228 (Stone et al. 1960).

229 The average size of the inversions fixed in *D. montana* was 10.7Mb and in *D. flavomontana* 9.4Mb (Fig.
230 3, Table S8), which resembles the average reported size of inversions in animals and plants (8.4Mb)
231 (Wellenreuther and Bernatchez 2018). Our finding of a larger number of inversions on the X is consistent
232 with theory showing that the fixation probability of X chromosomal inversions is higher than that of
233 autosomal inversions, because selection can more effectively favour beneficial and purify deleterious
234 recessive X-linked alleles than autosomal ones (Charlesworth et al. 1987; Vicoso and Charlesworth 2006;
235 Charlesworth et al. 2018; Connallon et al. 2018).

236 The polytene chromosomes studies by Stone et al. (1960) and Throckmorton (1982) suggest that *D.*
237 *montana* and *D. flavomontana* carry additional inversions that were not detected in this study. In
238 particular, *D. flavomontana* may harbour one fixed inversion of unknown size on the 3rd chromosome
239 (inversion E; Stone et al. 1960), which we might have missed due to the higher fragmentation of this
240 chromosome compared to the other chromosome contigs (Table S9). Given our limited sample size and
241 explicit focus on fixed inversion differences between species, polymorphic inversions previously found
242 in these species (Stone et al. 1960), which may be associated with local adaptation or other evolutionary
243 processes (Fang et al. 2012; Kapun et al. 2016; Wallberg et al. 2017), were also not identified here.

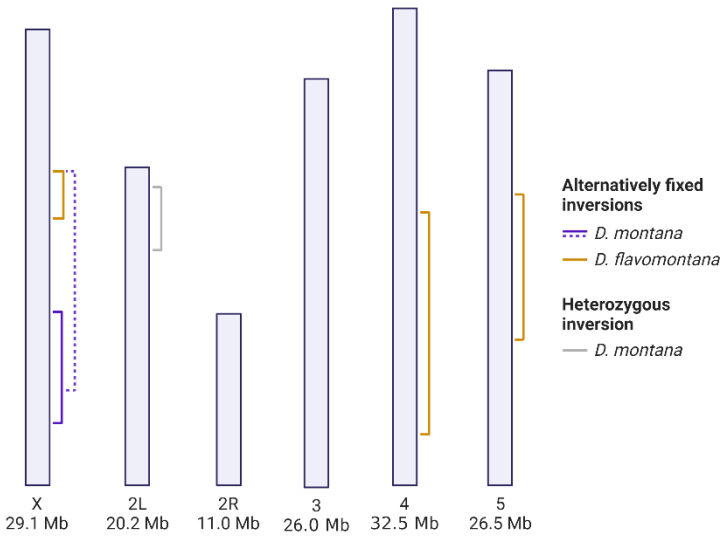

Figure 3. Chromosomes and five large (>0.5Mb) alternatively fixed inversions of *D. montana* (blue solid and dashed lines) and *D. flavomontana* (orange solid lines), as well as one heterozygous inversion of *D. montana* (light grey solid line) (Table S8). The numbers below each chromosome refer to its length in the *D. montana* assembly. Chromosome 2 has left (2L) and right (2R) arms that are separated by a submetacentric centromere.

Genetic divergence between *D. montana* and *D. flavomontana* is greater inside than outside inversions

We analysed the mean genetic divergence (d_{XY}) to test whether inversions have reduced recombination and introgression between *D. montana* and *D. flavomontana*, and if so, whether this is ancient or recent. In the latter case, d_{XY} should be lower in sympatry compared to allopatry (Noor and Bennett 2009; Harrison and Larson 2014). We estimated d_{XY} separately for coding, intronic and intergenic sequences and inverted and colinear regions of the genome. Given the potentially different evolutionary history of the X chromosome and the autosomes (Vicoso and Charlesworth 2006; Charlesworth et al. 2018), analyses for the X were performed separately. We also carried out separate analyses for allopatric and sympatric comparisons of the species.

Mean divergence (d_{XY}) between *D. montana* and *D. flavomontana* was remarkably similar for intergenic and intronic sequences but much lower for coding sequences (Fig. 4), as expected given the stronger selective constraint on coding sites (Halligan and Keightley 2006). Moreover, d_{XY} was slightly, but consistently lower for sympatric compared to allopatric comparisons of the species across all chromosome regions (Fig. 4, Table S10).

At non-coding sequences (i.e. intergenic and intronic), mean d_{XY} was consistently higher in inverted compared to colinear regions in allopatric and sympatric comparisons (Fig. 4, Table S10). At coding sequences, mean d_{XY} was increased for inversions on the 4th and the X chromosome compared to colinear regions both in allopatric and sympatric comparisons (Fig. 4, Table S10). Plotting d_{XY} in sliding

267 windows showed an increase in genetic divergence, especially around the inversion breakpoints and for
268 overlapping X inversions, for interspecific, but not for intraspecific comparisons (Fig. 5).

269 Overall, our finding of higher genetic divergence inside compared to outside of inversions is consistent
270 with the idea that inversions suppress gene exchange and facilitate the accumulation of genetic
271 differences (Fig. 4; Navarro and Barton 2003; Kirkpatrick and Barton 2006). We also found that genetic
272 divergence was highest around inversion breakpoints and in the series of overlapping inversions on the
273 X (Fig. 5), where recombination is the most suppressed (Hoffmann and Rieseberg 2008). Similar
274 signatures of elevated genetic divergence between closely related species inside and around inversion
275 breakpoints have been detected e.g. in other *Drosophila* species pairs (Noor et al. 2007; Kulathinal et
276 al. 2009; Lohse et al. 2015), *Helianthus* sunflowers (Barb et al. 2014), *Sorex* shrews (Basset et al. 2006),
277 and *Anopheles* mosquito (Michel et al. 2006). Finally, our finding of lower genetic divergence in
278 sympatry compared to allopatry (Fig. 4) is consistent with low levels of recent introgression in sympatry
279 (Noor and Bennett 2009; Harrison and Larson 2014).

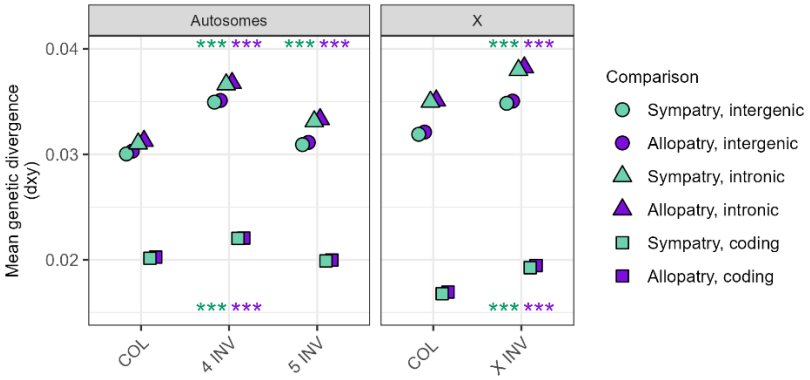

280

281 Figure 4. Mean genetic divergence (measured as d_{XY}) at intergenic, intronic and coding sequences of colinear (COL,
282 background) and inverted (INV) chromosome partitions on the autosomes and the X. Divergence are shown for
283 allopatric (purple) and sympatric (green) comparisons of *D. montana* and *D. flavomontana*. Significance levels
284 were inferred from simulations, where colinear (COL) regions were compared to inverted (INV) regions separately
285 for autosomes and the X chromosome, for intergenic, intronic and coding sequences, and for allopatric and
286 sympatric comparisons (*** $P < 0.001$; P-values for intergenic and intronic sequences shown above and for coding
287 sequences below dots; Table S10).

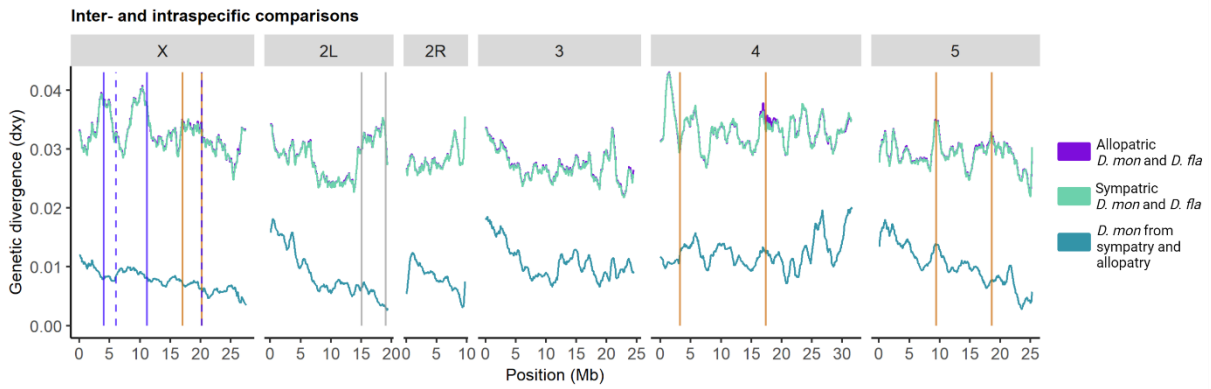

Figure 5. Genetic divergence (measured as d_{XY}) across the genome (including coding, intronic and intergenic regions) in sliding windows for allopatric and sympatric comparisons of *D. montana* and *D. flavomontana* (interspecific), and for *D. montana* originating from allopatry and sympatry (intraspecific). Vertical lines represent breakpoints of different inversions (see Fig. 3): blue solid and dashed lines, and orange solid lines indicate alternatively fixed inversions of *D. montana* and *D. flavomontana*, respectively, and grey solid lines indicate heterozygous *D. montana* inversion.

Hierarchical model comparison suggests species diverge with very low levels of post-divergence gene flow from *D. montana* to *D. flavomontana*

We used gIMble (Laetsch et al. 2022), an analytic likelihood method, to fit a series of demographic models of species divergence with and without long-term post-divergence gene flow, i.e. isolation with migration (IM) and strict divergence (DIV) models (Fig. 7), to the data summarised in terms of the bSFS (see Methods). The evolutionary history of the X chromosome (Vicoso and Charlesworth 2006; Charlesworth et al. 2018) and inversions (Lohse et al. 2015; Fuller et al. 2018) may differ from other chromosome regions, and these genomic partitions were therefore analysed separately from colinear, autosomal regions. To minimize the effects of selection, our initial analysis was limited to intergenic sequences of the colinear autosomal regions (repetitive regions were excluded). We performed separate analyses for sympatric and allopatric comparisons of *D. montana* and *D. flavomontana*. To evaluate the timing of potential recent introgression in sympatry compared to allopatry, we also performed a separate analysis for intraspecific comparison of *D. montana* (*D. montana* living in contact vs in isolation with *D. flavomontana*). We carried out this initial model comparison for the DIV and two IM models four times, using both *D. montana* and *D. flavomontana* as a reference genome to evaluate the potential effects of reference bias, and performed separate analyses for two different block lengths (64bp and 128bp). Parameter estimates and support values (lnCL) under all demographic models are shown in Table 2 for 64 bp blocks and using *D. montana* as a reference. Analogous analyses for all four combinations of block length and reference genomes are given in Table S11.

For both allopatric and sympatric comparisons and for three of the four combinations of block lengths and reference genomes used, the best-fitting demographic scenario was an IM model assuming introgression from *D. montana* into *D. flavomontana* (Table 2 & S11). Our parametric bootstrap analyses showed that the improvement in fit of this IM model compared to the DIV model was significant suggesting a low but genuine signal of introgression (Fig. S5 & S6). The only exception was the analysis using shorter 64bp blocks and *D. flavomontana* as a reference genome. In this case, the DIV model could not be rejected (Fig. S6). However, estimates for all parameters (T and N_es) were extremely similar regardless of the model (DIV and IM), block size (64bp and 128bp) and reference genome (*D. montana* and *D. flavomontana*) used (Table S11). Given the overall support for post-divergence gene flow and inherent bias of multilocus inference to underestimate migration, we assume an IM model with migration from *D. montana* into *D. flavomontana* as the best-fitting / most plausible scenario throughout for all subsequent analyses (Table 2). Yusuf et al. (2022) also recently found signatures of introgression between *D. montana* and *D. flavomontana* using a different approach, which gives further support for our introgression signal.

In contrast, for the intraspecific comparison of *D. montana*, the DIV model could not be rejected in any analysis. When using 64bp blocks, DIV and IM models had equal support, irrespective of which species was used as a reference (Table 2 & S11). Analyses based on longer 128bp blocks estimated slightly higher support for an IM model assuming post-divergence gene flow from allopatric (Alaskan) *D. montana* to sympatric (coastal/mountain) *D. montana* (Table 2 & S11). However, the parametric bootstrap analyses showed that the improvement in fit compared to the simpler DIV model was non-significant (Fig. S5 & S6). Consequently, the subsequent intraspecific analyses were conducted using the DIV model (Table 2).

Table 2. Support (measured as ΔlnCL) and parameter estimates for divergence time (*T* in years/generations), migration rate (*m*) and effective population sizes (N_e) for studied populations and their common ancestral population under strict divergence (DIV, *m*=0) and isolation with migration (IM) models with both gene flow directions. The model comparison is based on 64bp blocks and the *D. montana* reference genome, and was performed for intergenic autosomal colinear regions to minimize the effects of selection. Grey shading indicates the best-fit model for each comparison.

Comparison	Model	*D. mon* Ne	*D. fla* Ne	Ancestral Ne	T	m	lnCL	ΔlnCL
Allopatric	DIV	693,000	395,000	1,464,000	2,379,000	-	-45651205	12869
	IM *D. mon --> D. fla*	705,000	382,000	1,403,000	2,539,000	1.09E-08	-45638336	0
	IM *D. fla --> D. mon*	692,000	396,000	1,457,000	2,398,000	1.21E-09	-45650952	12616
Sympatric	DIV	720,000	392,000	1,459,000	2,343,000	-	-136875659	47790
	IM *D. mon --> D. fla*	735,000	377,000	1,388,000	2,526,000	1.29E-08	-136827869	0
	IM *D. fla --> D. mon*	719,000	393,000	1,447,000	2,376,000	2.13E-09	-136873722	45853
	Model	***D. mon allop* Ne**	***D. mon symp* Ne**	**Ancestral Ne**	**T**	**m**	**lnCL**	**ΔlnCL**
Intraspecific	DIV	1,087,000	1,560,000	858,000	210,000	-	-39887382	0
	IM *D. mon symp. --> D. mon allop.*	1,087,000	1,560,000	858,000	210,000	1.50E-15	-39887382	0
	IM *D. mon allop. --> D. mon symp.*	1,079,000	1,441,000	858,000	217,000	3.32E-07	-39887408	27

343 Species-specific inversions were fixed earlier or around the species' split and introgression was lower
344 inside compared to outside of inversions and in allopatry compared to sympatry

345 We used the best-fit isolation with migration (IM) model (Table 2) to examine the potential role of
346 inversions and introgression in the speciation history of *D. montana* and *D. flavomontana*. As before, all
347 analyses were limited to intergenic regions to minimize the effects of selection, and separate analyses
348 were carried out for the X chromosome and autosomes, for inverted and colinear regions, and for
349 sympatric and allopatric populations of the species. To estimate the timing of potential recent
350 introgression, we analysed the split time for *D. montana* living in contact (sympatry) or in isolation
351 (allopatry) with *D. flavomontana* using the simpler strict divergence (DIV) model (intraspecific
352 comparison; Table 2).

353 Taking the estimates for the colinear autosomal background as face value, *D. montana* and *D.*
354 *flavomontana* have diverged ca 2.5 Mya (Table 3, Fig. 6A & 6C). The divergence time estimates of the
355 inversions differ from each other, and the inversions on the 4th, 5th and the X chromosome predate the
356 divergence time estimated for the colinear background (ca 2.8-3.3 Mya) (Table 3, Fig. 6A & 6C). For all
357 chromosome partitions, genetic diversity (π) and the effective population size (N_e) of *D. montana* were
358 approximately two times as large as those of *D. flavomontana* (Table 3, Fig. S7). *D. montana* populations
359 living in contact (sympatry) and in isolation (allopatry) with *D. flavomontana* have diverged
360 approximately 210 000 years ago (Table 3, Fig. 6C), an order of magnitude more recent than the split
361 between *D. montana* and *D. flavomontana*.

362 Estimated long-term gene flow from *D. montana* to *D. flavomontana* were lower inside than outside of
363 inversions both on the autosomes and the X (Table 3, Fig. 6B), which is in accordance with the finding
364 that genetic divergence of non-coding (intergenic and intronic) sequences was consistently higher inside
365 than outside of inversions (Fig. 4, Table S10). Moreover, migration rate estimates were higher in
366 sympatry compared to allopatry (Table 3, Fig. 6B), which again agrees with the slightly, but consistently
367 lower genetic divergence in sympatric compared to allopatric comparisons of the species (Fig. 4, Table
368 S10).

Table 3. Parameters for effective populations sizes, divergence time (*T* in years/generations), and migration rate (*M*) estimated from 64bp blocks under the $IM_{mon \rightarrow fla}$ model for allopatric and sympatric comparisons and under the DIV model for intraspecific comparison.

Comparison	Genomic region		Ne ancestral	Ne *D.mon*	Ne *D. fla*	T	M
Allopatry	Autosomes	COL	1,403,000	705,000	382,000	2,539,000	0.0083
		4 INV	1,644,000	798,000	474,000	2,941,000	0.0049
		5 INV	1,364,000	718,000	396,000	2,777,000	0.0060
	X	COL	1,700,000	443,000	225,000	2,605,000	0.0074
		X INV	1,904,000	441,000	368,000	2,829,000	0.0038
Sympatry	Autosomes	COL	1,388,000	735,000	377,000	2,526,000	0.0097
		4 INV	1,603,000	865,000	470,000	2,988,000	0.0067
		5 INV	1,321,000	752,000	392,000	2,823,000	0.0076
	X	COL	1,592,000	493,000	219,000	2,769,000	0.0088
		X INV	1,591,000	607,000	365,000	3,321,000	0.0078
Comparison	**Genomic region**		**Ne ancestral**	**Ne allop *D. mon***	**Ne symp *D. mon***	**T**	
Intraspecific	Autosomes	COL	858,000	1,087,000	1,560,000	210,000	

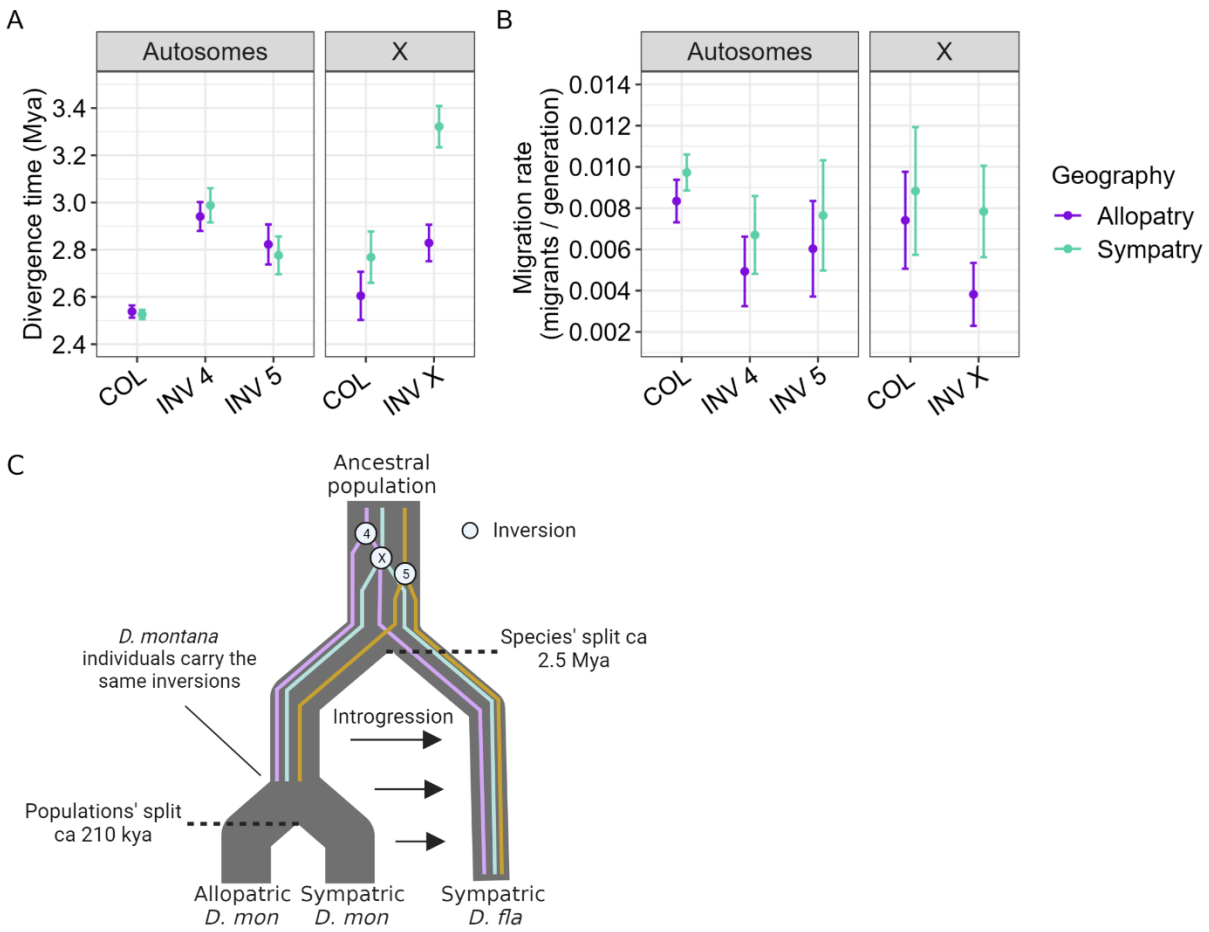

Figure 6. Estimates of (A) split times and (B) migration rates between *D. montana* and *D. flavomontana* for different chromosome partitions and for allopatric (purple) and sympatric (green) comparisons. Confidence intervals were estimated using a parametric bootstrap as +/- 2 SD across 100 datasets simulated under the best-fit IM model with recombination (see Methods). (C) Illustration of the likely evolutionary history of *D. montana* and *D. flavomontana*.

379 Taken together, our analyses suggest that *D. montana* and *D. flavomontana* diverged ca 2.5 Mya from
380 a large ancestral population, which is broadly compatible with a recent estimate of 3.8 Mya based on
381 small introns and the same molecular clock calibration (Yusuf et al. 2022). Crucially, split time estimates
382 for all five fixed inversions we have identified on the X, 4th and 5th chromosome predate the estimated
383 species split time based on the colinear background, and so, these inversions must have existed already
384 in the common ancestral population. In other words, we can rule out the possibility that the inversions
385 arose after the onset of species divergence (in which case we would expect identical divergence time
386 estimates). The reduced introgression for inversions compared to colinear regions we have estimated
387 is a clear and expected consequence of reduced recombination and gene flow between alternative
388 arrangements at each inversion.

389 What is less clear, is the extent to which local adaptation in the face of gene flow in the ancestral
390 population facilitated the fixation of these inversions (and vice versa) or whether the fixed inversions
391 are a mere byproduct of population processes unrelated to speciation. The fact that three fixed
392 inversions on the X are i) overlapping and ii) associated with a strong incompatibility preventing
393 introgression from *D. montana* to *D. flavomontana* across the entire X chromosome (Poikela et al. 2022)
394 suggests that these inversions have indeed contributed to the build-up of reproductive isolation and
395 acted as barriers to gene flow early on in the speciation process (Noor and Bennett 2009; Fuller et al.
396 2018). In contrast, we have no evidence that the inversions on the 4th and 5th chromosomes are
397 enriched for BDMIs (Poikela et al. 2022) or loci under divergent selection, so we cannot rule out a
398 scenario in which these inversions have been maintained in the ancestral populations by balancing
399 selection (as seems to be the case for inversion 2L in *D. montana*) and become fixed between *D.*
400 *montana* and *D. flavomontana* simply by chance (Guerrero and Hahn 2017). However, even for the X
401 inversions we cannot verify whether the associated incompatibility allele(s) arose before or around the
402 species' split, or afterwards (post-speciation event).

403 Although we find evidence for post-divergence gene flow, it is worth highlighting that our estimate of
404 long-term rate of migration from *D. montana* to *D. flavomontana* is extremely small compared to
405 analogous estimates for other young *Drosophila* sister species (Lohse et al. 2015); e.g. *D. mojavensis*
406 and *D. arizonae* have approximately one migrant per generation, while our estimate for *D. montana* and
407 *D. flavomontana* is roughly 1 migrant in 80 generations, two orders of magnitude lower. Thus, even the
408 total probability of a lineage sampled in *D. flavomontana* to trace back to *D. montana* via migration (1-
409 e^(-T M)) is only 3.2%. This low rate of long-term effective migration agrees well with our previous
410 evidence for strong pre- and postzygotic barriers between the species (Poikela et al. 2019). In addition,
411 the species' differences in the usage of host trees (Throckmorton 1982) and the ability to tolerate cold
412 (Poikela et al. 2021) might have contributed to ecological isolation and reduced their encounters in

413 nature. Intriguingly, we found higher levels of introgression in sympatry compared to allopatry, which
414 suggests at least some introgression from *D. montana* to *D. flavomontana* over the past ~210 000 years,
415 i.e. after the allopatric (Alaskan) *D. montana* populations diverged from *D. montana* coexisting with *D.*
416 *flavomontana*. Already low levels of introgression and selection against introgressed ancestry in the new
417 genetic background may facilitate reinforcement of prezygotic barriers to prevent maladaptive
418 hybridization between species, and eventually complete the speciation process (Servedio and Noor
419 2003; Cruickshank and Hahn 2014). This is consistent with our previous finding that *D. flavomontana*
420 has developed stronger prezygotic barriers against *D. montana* in sympatry compared to allopatry,
421 presumably as a result of reinforcement (Poikela et al. 2019).

422 Our demographic inferences are limited in several ways. Firstly, the IM model is overly simplistic in
423 assuming an instantaneous onset of species divergence and a constant rate of introgression throughout
424 the species' evolutionary history. However, given the overall extremely low estimate of gene flow and
425 the computational limitations of gIMble, we have not attempted to fit – and can therefore not exclude
426 − more realistic (but necessarily more complex) demographic scenarios of either historical gene flow
427 which reduced due to the emergence of strong barriers or sudden discrete bursts of admixture following
428 periods of complete isolation. Secondly, our inference ignores recombination within blocks, a
429 simplifying assumption that is known to lead to biased parameter estimates (Wall 2003). In particular,
430 we found that the estimates of *T* obtained from parametric bootstrap replicates (simulated with
431 recombination) are substantially larger (~3.4 MY) than the true values (Table 3, Fig. 6 & S8), which
432 suggests that we have overestimated species divergence time overall. Finally, our approach of fitting an
433 IM model to inverted regions ignores the fact that inversions arise in a single individual and may be fixed
434 in a selective sweep. An inversion arising and sweeping to fixation immediately after the onset of species
435 divergence would result in a lower estimate of N_e for the species in which they fixed. If anything, we see
436 the opposite pattern: i.e. larger estimates of *D. flavomontana* N_e for the inversions on the 4th and 5th
437 chromosome compared to the colinear background (Table 3), which is again compatible with an
438 inversion origin in the ancestral population before the estimated species split. It is striking that all
439 inversions date to a short interval just before the species split (~600k years/generations) which is the
440 same order as the (ancestral) population size. Given that we infer a substantially larger effective size for
441 the ancestral population than fo*r D. montana* and *D. flavomontana*, one could interpret the interval in
442 the ancestral population in which the inversions arose as the period of (rather than before) speciation.

443 Even though many species pairs differ from each other by multiple inversions, the majority of inversion
444 differences must have arisen after speciation (Faria and Navarro 2010). Performing pairwise
445 comparisons for younger and older species would offer a more holistic view of the role of inversions in
446 speciation events. In our case, characterizing inversions and investigating divergence times and

447 introgression across all species of the *montana* phylad of the *virilis* group (*D. montana*, *D. flavomontana*,
448 *D. borealis* and *D. lacicola*) (Hoikkala and Poikela 2022) could provide valuable additional information.
449 In general, investigating millions of years old events by fitting necessarily drastically simplified scenarios
450 of reality involve uncertainties. Experimental approaches, potentially with the help of CRISPR/Cas9 gene
451 editing technique, could allow the creation of artificial inversions or reversion of existing ones, and direct
452 tests of the role of inversions in speciation (Faria and Navarro 2010; Faria et al. 2018; Hopkins et al.
453 2020; White et al. 2020).

454 Conclusions

455 It has proven extremely difficult to test if and how inversions facilitate speciation, and empirical
456 evidence on the role of inversions in speciation is largely lacking (Faria and Navarro 2010; Fuller et al.
457 2019). We explored these questions in two sister species of the *D. virilis* group, *D. montana* and *D.*
458 *flavomontana*. Our main goals were (1) to characterize alternatively fixed chromosomal inversions of *D.*
459 *montana* and *D. flavomontana*, (2) to investigate the age of the inversions, and (3) to identify whether
460 the inversions have restricted gene exchange between *D. montana* and *D. flavomontana*, and either
461 protected existing genetic incompatibilities in the secondary contact, or facilitated the accumulation of
462 incompatibilities in the presence of gene flow.

463 Taking advantage of long- and short-read genome sequencing technologies, we generated the high-
464 quality contiguous reference assemblies for *D. montana* and *D. flavomontana*. These genomes enabled
465 us to accurately characterize inversions that are alternatively fixed between these sister species across
466 their distribution area in North America. We were able to assign the majority of these to inversions that
467 were described for the species already in the 1950s and 1960s based on polytene chromosome studies
468 (Stone et al. 1960). Our analyses show that the inversions on the 4th, 5th and the X chromosome arose
469 before the onset of species divergence. Thus, the elevated genetic divergence inside compared to
470 outside of inversions results most likely from restricted recombination and gene flow between locally
471 adapted populations of the ancestral form. However, only the X inversions have been found to contain
472 strong BDMI(s) that effectively restricts introgression from *D. montana* to *D. flavomontana* across the X
473 chromosome in the first few backcross generations (Poikela et al. 2022), and provide evidence for the
474 enrichment of BDMIs within inversions. Accordingly, our results support the idea that ancestrally
475 polymorphic inversions, particularly the X chromosomal inversions in our case, can drive the speciation
476 process by aiding the accumulation of genetic divergence and incompatibilities (Fuller et al. 2018), while
477 colinear regions keep exchanging genetic material until strong reproductive isolation has formed.

478 Even though the estimates of introgression between the species were extremely low, *D. flavomontana*
479 has experienced some introgression from *D. montana* over the past ~210 000 years in sympatric

480 populations of the species. In general, selection can strengthen prezygotic barriers between species in
481 response to low levels of poor functioning introgressed alleles, which likely leads to the strengthening
482 of overall reproductive isolation and the completion of the speciation process (Servedio and Noor 2003;
483 Cruickshank and Hahn 2014). This agrees with our previous evidence on *D. flavomontana* having
484 developed stronger prezygotic barriers against *D. montana* in sympatric compared to allopatric
485 populations of the species, potentially as a result of reinforcement (Poikela et al. 2019).

486 Overall, our study suggests that inversions may indeed be early triggers in the speciation process and
487 highlights the value of interpreting the evolutionary effects of inversions through the lens of
488 demographic models. However, in doing so, we have ignored much of the mechanistic and selective
489 details of inversion evolution. Regions with repetitive sequences, such as transposable elements, tRNAs,
490 ribosomal genes or segmental duplications, are prone to breakage and are often the initial source of an
491 inversion (Kapun and Flatt 2019). Investigating repetitive sequences or small structural variations
492 around the inversion breakpoints would increase our understanding on how the inversions originated
493 in the first place. Moreover, inversions are not static through their lifetime, but evolve in response to
494 changes in selection, genetic drift, new mutations and gene flux (occurring via double cross-overs and
495 gene conversion), as well as by interactions with colinear genome or with other inversions (Faria et al.
496 2018). Given the many, sometimes entangled processes affecting the origin and the fixation of
497 inversions, models that can extract information about both demography and the selective forces acting
498 on inversions in the early stages of speciation are the next obvious step in understanding how inversions
499 facilitate the origin of species (Faria et al. 2018).

500 ## Materials and Methods

501 ### Sample collections and maintenance

502 *D. montana* and *D. flavomontana* females were collected from several sites in the Rocky Mountains and
503 along the western coast of North America, and Alaska 2013–2015 (Fig. 1, Table S1). Sites in the Rocky
504 Mountains and the western coast of North America are either inhabited by both species (sympatric
505 sites: Jackson, Cranbrook, McBride, Terrace, Vancouver, Ashford, Fall Creek), or by one of the species
506 with nearby sites inhabited by both species (parapatric sites: Liberty, Afton, Livingston, Azalea) (Fig. 1,
507 Table S1). *D. montana* also has stable populations in high latitudes in Alaska, where *D. flavomontana*
508 does not exist. We refer to the comparisons between *D. montana* and *D. flavomontana* from the Rocky
509 Mountains and from the western coast as "sympatry", and those between *D. montana* from Alaska and
510 *D. flavomontana* from the Rocky Mountains or the western coast as "allopatry" (Fig. 1). Intraspecific
511 comparison was performed for *D. montana* living in isolation (allopatry) and in contact (sympatry) with
512 *D. flavomontana* (Fig. 1).

513 The newly collected females were brought to the fly laboratory, with a constant light, 19±1 ˚C and ~60%
514 humidity, at the University of Jyväskylä, Finland. Females that had mated with one or several males in
515 nature were allowed to lay eggs in malt vials for several days, after which they were stored in 70% EtOH
516 at -20 ˚C. The emerged F_1 progeny of each female were kept together to produce the next generation
517 and to establish isofemale strains. After that also the F_1 females were stored in 70% EtOH at -20 ˚C.

518 ### DNA extractions and sequencing

519 We performed PacBio long-read sequencing from two *D. montana* and two *D. flavomontana* isofemale
520 strains that had been kept in the fly laboratory since their establishment (Fig. 1, Table S1). DNA of the
521 Seward *D. montana* and both *D. flavomontana* samples were extracted from a pool of 60 three days old
522 females per isofemale strain using cetyltrimethylammonium bromide (CTAB) solution with RNAse
523 treatment, Phenol-Chloroform-Isoamyl alcohol (25:24:1) and Chloroform-Isoamyl alcohol (24:1)
524 washing steps, and ethanol precipitation at the University of Jyväskylä, Finland. DNA of the Jackson *D.*
525 *montana* sample was extracted with the "DNA Extraction SOP For Animal Tissue" protocol and purified
526 with Ampure beads at BGI (Beijing Genomics Institute). Quality-checked DNA extractions of the Seward
527 *D. montana* sample and both *D. flavomontana* samples were used to generate >15kb PacBio libraries,
528 which were all sequenced on two SMRT cells within a PacBio Sequel system (Pacific Biosciences, United
529 States) at the Norwegian Sequencing Centre in 2018. DNA of the Jackson *D. montana* sample was used
530 to generate >20kb PacBio libraries and was sequenced on one SMRT cell using the PacBio Sequel system
531 at BGI in 2019. Average PacBio raw read coverage was 27-35X per sample, except for the Jackson *D.*

532 *montana* sample which was sequenced at 77X coverage. Detailed information on the PacBio raw reads
533 of each sample is provided in Table S2.

534 We generated Illumina re-sequencing data for 12 *D. montana* and 9 *D. flavomontana* single wild-caught
535 females or their F_1 daughters from several locations in North America (Fig. 1, Table S1). DNA extractions
536 were carried out at the University of Jyväskylä, Finland, using a CTAB method as described above.
537 Quality-checked DNA extractions were used to produce an Illumina library for each sample in three
538 batches. First, Nextera libraries were used to generate 150bp paired-end (PE) reads on two lanes using
539 HiSeq4000 Illumina instrument at Edinburgh Genomics in 2017. Second, one Truseq library was used to
540 generate 150bp PE reads on one lane of a HiSeq4000 Illumina instrument at the Norwegian Sequencing
541 Centre in 2018. Third, Truseq libraries were used to generate 150bp PE reads on one lane of a HiSeq X-
542 Ten Illumina instrument at BGI in 2019. We generated on average 46-95X coverage per sample, except
543 for the *D. montana* sample from Seward, which was sequenced to 371X coverage. Detailed information
544 on Illumina raw reads is provided in Table S2.

545 Genome assemblies and scaffolding

546 We generated initial *de novo* assemblies for each PacBio dataset and the respective Illumina reads using
547 the wtdbg2 pipeline v2.5 (RedBean; Ruan & Li, 2020) and MaSuRCA hybrid assembler v3.3.9 (Zimin et
548 al., 2017). To improve assembly contiguity, we used quickmerge for both assemblies of each sample
549 (Chakraborty et al. 2016). The initial assembly statistics are given in Table S12. We polished the resulting
550 assemblies with the respective Illumina reads using Pilon v1.23 (Walker et al. 2014) and removed
551 uncollapsed heterozygous regions using purge_dups (Guan et al. 2020).

552 We identified genomic contaminants in the assemblies with BlobTools v1.1 (Laetsch and Blaxter 2017).
553 PacBio and Illumina reads were first mapped back to each assembly with minimap2 (Li, 2018) and BWA
554 mem (Burrows-Wheeler Aligner) v0.7.17 (Li & Durbin, 2009), respectively. Contigs in the assemblies
555 were then partitioned into taxonomic groups based on similarity search against the NCBI nucleotide
556 database (BLASTn 2.9.0+; Camacho et al., 2009) and Uniref90 (Diamond v0.9.17; Buchfink, Xie, & Huson,
557 2015). Finally, contigs were visualized on a scatter plot and coloured by putative taxonomic groups (Fig.
558 S1-S4). Non-Diptera contigs were removed manually from the assemblies based on sequence GC
559 content, read coverage and taxonomy assignment. We estimated the completeness of the assemblies
560 with the BUSCO pipeline v5.1.2 using the Diptera database "diptera_odb10" (Seppey et al. 2019), which
561 searches for the presence of 3285 conserved single copy Diptera orthologues.

562 We constructed chromosome-level reference genomes for both species by scaffolding contigs of the
563 original assemblies with a reference-genome -guided scaffolding tool RagTag v2.1.0 (Alonge et al.,
564 2019), which orients and orders the input contigs based on a reference using minimap2 (Li 2018). We

565 used default settings except for the increased grouping confidence score (-i) which was increased to
566 0.6. For *D. montana*, we scaffolded the Seward *D. montana* assembly with the *D. lummei* genome
567 (Poikela et al. in prep.), which was constructed using PacBio and Illumina reads and assigned to
568 chromosomes using the published *Drosophila virilis* chromosome map (Schäfer et al. 2010) and *D. virilis*
569 assembly dvir_r1.03_FB2015_02 obtained from Flybase. For *D. flavomontana*, we first scaffolded the
570 Livingston *D. flavomontana* assembly with the Vancouver *D. flavomontana* assembly and then with *D.*
571 *lummei*. In *D. montana* and *D. flavomontana*, chromosome 2 has right (2R) and left (2L) arms, separated
572 by a (sub)metacentric centromere, whereas in other *virilis* group species the centromere is located near
573 one end of the chromosome 2 (Stone et al. 1960). Therefore, scaffolding of chromosomes 2L and 2R
574 was not feasible with the *D. lummei* genome.

575 For the *D. montana* chromosome-level reference genome, the X (29.1Mb), 2L (20.2Mb) and 2R (11.0Mb)
576 chromosomes could not be further scaffolded, while the lengths of chromosomes 3, 4 and 5 were
577 increased substantially by scaffolding. The longest contig of chromosome 3 increased from 5.8Mb to
578 26.0Mb (constructed from 37 contigs), chromosome 4 from 12.3Mb to 32.5Mb (28 contigs), and
579 chromosome 5 from 19.5Mb to 26.5Mb (11 contigs; Table S3). For the *D. flavomontana* chromosome-
580 level reference genome, the X chromosome (29.0Mb) could not be further scaffolded, while the lengths
581 of all other chromosomes increased due to scaffolding. Chromosome 2L increased from 10.2Mb to
582 20.4Mb in length (3 contigs), 2R from 10.4Mb to 10.6Mb (3 contigs), the 3rd chromosome from 7.8Mb
583 to 24.5Mb (33 contigs), the 4th chromosome from 20.0Mb to 30.7Mb (14 contigs), and the 5th
584 chromosome from 23.5Mb to 27.2Mb (4 contigs; Table S3).

585 Genome annotations

586 All genome assemblies were annotated for repetitive regions and genes. *De novo* libraries of repeat
587 sequences were built for each assembly using RepeatModeler v2.0.1 (Flynn et al. 2019), and repetitive
588 regions were softmasked, together with *Drosophila*-specific repeats (Dfam_3.1 (Hubley et al. 2016) and
589 RepBase-20181026 (Bao et al. 2015), using RepeatMasker v4.1.0 (Smit et al. 2013-2015). Gene models
590 were predicted on the softmasked assemblies of *D. montana* using the BRAKER2 pipeline. For gene
591 annotation, we used RNA-seq data (Illumina Truseq 150bp PE) from whole-body female and male *D.*
592 *montana* adult flies collected in Finland (Parker et al. 2021). RNA-seq reads were trimmed for adapter
593 contamination and read quality using fastp v0.20.0 (Chen et al. 2018), and mapped to both softmasked
594 *D. montana* assemblies using STAR v2.7.0 (Dobin et al. 2013). Finally, *D. montana* gene annotations were
595 carried out with BRAKER2s ab initio gene prediction pipeline with RNA-seq evidence using Augustus
596 v3.3.3 and GeneMark-ET v4.48 (Stanke et al. 2006; Stanke et al. 2008; Li et al. 2009; Barnett et al. 2011;
597 Lomsadze et al. 2014; Hoff et al. 2016; Hoff et al. 2019). Protein predictions of the Jackson *D. montana*

598 assembly with the best BUSCO values (see the Results) were used to annotate both *D. flavomontana*
599 and both chromosome-level genomes using the BRAKER2s ab initio gene prediction pipeline with
600 GenomeThreader and AUGUSTUS (Stanke et al. 2006; Stanke et al. 2008; Gremme 2013; Buchfink et al.
601 2014; Hoff et al. 2016; Hoff et al. 2019). Annotation completeness was assessed using BUSCO v5.1.2
602 against the 'diptera_odb10' database (Seppey *et al.* 2019).

603 Mapping, variant calling and variant filtering

604 To investigate genome-wide variation in sympatric and allopatric populations of the species, we mapped
605 all Illumina samples to the *D. montana* chromosome-level assembly. For this, we quality-checked
606 Illumina PE reads of each sample with FastQC v0.11.8 (Andrews 2010) and trimmed them for adapter
607 contamination and low-quality bases using fastp v0.20.0 (Chen et al. 2018). We mapped each trimmed
608 Illumina sample against the genome using BWA mem v0.7.17 with read group information (Li and Durbin
609 2009), sorted alignments with SAMtools v1.10 (Li et al. 2009) and marked PCR duplicates with
610 sambamba v0.7.0 (Tarasov et al. 2015). The resulting BAM-files were used for variant calling with
611 freebayes v1.3.1-dirty (Garrison and Marth 2012). Raw variants were processed with gIMble preprocess
612 (genome-wide IM blockwise likelihood estimation toolkit; Laetsch et al. 2022). In brief, non-SNP variants
613 were deconstructed into allelic primitives, where remaining non-SNPs were removed in addition to any
614 SNP variant within two bp of a non-SNP. Genotype calls of remaining SNP variants were set to missing if
615 any of the following assumptions was violated: i) sample depth (FMT/DP) between 8 and 2SD from the
616 mean coverage, ii) read directionality placement balance (RPL>=1, RPR>=1), or iii) read strand placement
617 balance (SAF>=1, SAR>=1).

618 Principal component analysis of SNP and climatic data

619 To group Illumina samples according to their species and population type, we performed a principal
620 component analysis (PCA) on the filtered VCF-file, including all samples, chromosomes, and coding,
621 intronic and intergenic SNPs using PLINK v1.9 package (Chang et al. 2015). The VCF-file was converted
622 to PLINK's BED/BIM format and the PCA was run with PLINK's --pca function.

623 We performed another PCA on the climatic variables at fly sampling sites to visualize the climatic
624 variation amongst them. First, we downloaded climatic information from WorldClim database v2.1
625 (2.5min spatial resolution, dataset 1970-2000; Fick and Hijmans 2017) using latitudinal and longitudinal
626 coordinates of each site (Table S1) and extracted 19 bioclimatic variables using the "raster" package
627 v2.8-19 (Hijmans and Etten 2020; Table S4, S5). We then performed PCA on the bioclimatic variables,
628 describing temperature and humidity conditions in each site. We performed the PCA using the
629 "FactoMineR" package (Lê et al. 2008) in R v3.4.3 and R studio v1.1.383.

630 Characterization of chromosomal inversions

631 We identified large (>500kb) alternatively fixed inversions between *D. montana* and *D. flavomontana*
632 using both long- and short-read data. First, we mapped PacBio reads of each sample against each of the
633 four assemblies using ngmlr v0.2.7 (Sedlazeck et al. 2018) and obtained structural variant (SV)
634 candidates from the SV identification software, Sniffles v1.0.12 (Sedlazeck et al. 2018). Second, we
635 mapped Illumina PE reads against each of the four assemblies as explained in the "Mapping, variant
636 calling and variant filtering" paragraph. The resulting BAM-files were given to Delly v0.8.1, which
637 identifies structural variants based on paired-end read orientation and split-read evidence (Rausch et
638 al. 2012). Third, we used SURVIVOR (Jeffares et al. 2017) to identify species-specific, geographically
639 widespread inversions that were shared by Sniffles and Delly outputs and that were found in at least in
640 9 *D. montana* (out of 12) and 6 *D. flavomontana* (out of 9) samples. Putative breakpoints of each
641 inversion were located within a single contig, except for the 4th chromosome inversion where
642 breakpoints were located in two different contigs (Table S8). This inversion was therefore verified by
643 mapping long- and short-read data against the *D. lummei* genome which has a more contiguous
644 chromosome 4 (Table S8). The putative breakpoints of all inversions were confirmed visually with
645 Integrative Genomics Viewer (IGV) v2.8.0 (Thorvaldsdóttir et al. 2013) using both long- and short-read
646 data (an example IGV view shown in Fig. S9). Finally, we determined whether the inversions belong to
647 *D. montana* or *D. flavomontana* by mapping *D. lummei* PacBio long-reads (Poikela et al., in prep.) against
648 each assembly.

649 Modelling divergence and post-divergence gene flow

650 We analysed mean genetic divergence (d_{XY}) and fitted models of species divergence with and without
651 long-term interspecific gene flow between and within the species using gIMble (Laetsch et al. 2022).
652 This analytic likelihood method uses the joint distribution of mutation types in short sequence blocks,
653 the blockwise site frequency spectrum (bSFS), across subsamples of pairs of individual genomes to fit a
654 series of models of speciation history. We summarised data by the bSFS for two block lengths, 64bp and
655 128bp.

656 Given the potentially different evolutionary history of the X chromosome and the autosomes (Vicoso
657 and Charlesworth 2006; Charlesworth et al. 2018), we ran separate analyses for them throughout.
658 Colinear regions, ending at inversion breakpoints, were combined across autosomes as these regions
659 are expected to share the same evolutionary history, while inversions from different chromosomes may
660 differ in age and were analysed separately. The overlapping inversions of the X chromosome were
661 analysed together following Counterman and Noor (2006) and Lohse et al. (2015). We analysed different
662 chromosome partitions separately for allopatric and sympatric comparisons of the species. We also

663 analysed the split time of *D. montana* populations living in isolation (allopatry) and in contact (sympatry)
664 with *D. flavomontana* to evaluate the timing of potential recent introgression between the two species.
665 The intraspecific divergence time was inferred from the colinear autosomal regions, i.e. the same data
666 partition we used to infer the interspecific background history.

667 We first calculated d_{XY} for different genomic regions (i.e. colinear and inverted autosomes, and colinear
668 and inverted X chromosome) and for allopatric and sympatric populations to evaluate the role of
669 inversions in suppressing gene exchange. These analyses were carried out separately for coding, intronic
670 and intergenic regions (repetitive regions were excluded from all data partitions). To test whether d_{XY}
671 was reduced within inversions, we simulated datasets corresponding in size to the data sampled for
672 each inversion under the background demography (inferred from colinear autosomal regions) and
673 compared the observed d_{XY} to the distribution. We simulated inversion datasets under a minimal,
674 conservative model of recombination, which allows for gene conversion but no cross-over. We assumed
675 a rate of (initiation of) gene conversion of 3.59×10^{-8} per bp per generation. This corresponds to recent
676 estimates for *Drosophila pseudoobscura* and *Drosophila persimilis* (1.4×10^{-5} converted sites per bp per
677 generation; mean GC tract length of 390bp) (Korunes and Noor 2018). We simulated sequences of
678 100kb in length, two orders of magnitude shorter than total length of intergenic sequence per inversion.

679 Before analysing different chromosome partitions, we investigated the likely evolutionary history of *D.*
680 *montana* and *D. flavomontana* by comparing the likelihood of different demographic models. We
681 limited this initial model selection of allopatric, sympatric and intraspecific comparisons to intergenic
682 sequences of colinear autosomal regions (repetitive regions excluded) to minimize the effects of
683 selection. The simplest, strict divergence (DIV) model considers isolation at time *T* without interspecific
684 gene flow, i.e. isolation in allopatry (Fig. 7A). The isolation with migration (IM) model allows
685 unidirectional migration rate at a constant rate *M* (Fig. 7B). The IM model was fitted to both gene flow
686 directions (i.e. from *D. montana* to *D. flavomontana* and from *D. flavomontana* to *D. montana*, and from
687 allopatric to sympatric *D. montana* and from sympatric to allopatric *D. montana*). The DIV and IM models
688 allow asymmetric effective population size (N_e) between the descendent populations, and a separate
689 N_e for the ancestral population. Analyses based on the bSFS assume a constant mutation rate (μ) across
690 blocks and no recombination within them. We assumed a mutation rate (μ) of 2.8×10^{-9} per site per
691 generation, based on an estimate of the spontaneous mutation rate in *Drosophila melanogaster*
692 (Keightley et al. 2014). The estimates of *T* are converted into absolute time using $t = T \times 2N_e \times g$, where
693 $N_e = \theta/(4\mu)$ and g is generation time. We assumed one generation per year, i.e. the generation time of
694 Alaskan *D. montana* populations and most likely that of the ancestral population of the species, even
695 though other *D. montana* and *D. flavomontana* populations presently have two generations per year
696 (Tyukmaeva et al. 2020). To consider the potential effects of reference bias, we performed model fitting

and selection twice using both *D. montana* and *D. flavomontana* chromosome-level assemblies as reference genomes.

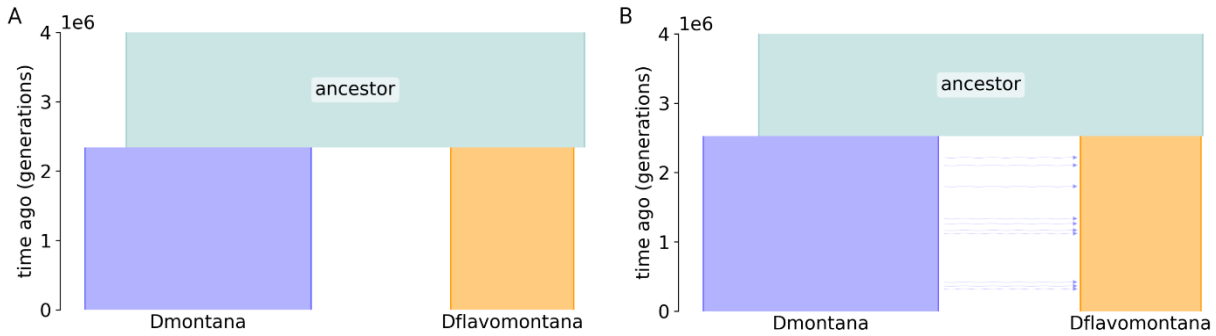

Figure 7. Sketches of the demographic models. The block widths indicate relative effective population sizes (N_e) of the ancestral population and its two descendants *D. montana* and *D. flavomontana*. (A) This model assumes no gene flow, i.e. strictly allopatric speciation (DIV). (B) The isolation with migration (IM) model allows unidirectional gene flow at rate *M* migrants per generation in this case from *D. montana* to *D. flavomontana*. Figures were produced with demesdraw (Gower et al. 2022).

To estimate the uncertainty in parameter estimates, i.e. the difference in support (ΔlnCL) between different demographic scenarios, we performed a parametric bootstrap. We used gIMble simulate to simulate 100 replicate datasets (of the same size as the real data in terms of numbers of blocks). To include the effect of linkage between blocks, we simulated data in 1000 chunks assuming a recombination rate of 8.9×10^{-9} calculated from the total map length (i.e. 1.76×10^{-8} divided by two given the absence of recombination in males). Specifically, we simulated data under the DIV model and fitted that model to the DIV and the best-fitting IM model to each replicate to obtain a null distribution of ΔlnCL between models (see Fig. S5 & S6).

Finally, to investigate the role of inversions in speciation, we performed demographic analyses under the best-fit model separately for different chromosome partitions (i.e. colinear and inverted autosomes, and colinear and inverted X chromosome) and for allopatric and sympatric comparisons of *D. montana* and *D. flavomontana*. The uncertainty in estimates of *T* and *M* for each data partition were inferred from 100 parametric bootstrap replicates/simulations.

Acknowledgements

We want to thank Anna-Lotta Hiillos and Jesse Mänttäri for their help with laboratory work and Edinburgh Genomics, Norwegian Sequencing Centre and BGI for sequencing the samples. This work was supported by the grant from Academy of Finland project 322980 to MK, and grant from Suomen Kulttuurirahasto (Keski-Suomen rahasto) to NP and MK. KL and DRL are supported by an ERC starting grant (ModelGenomLand, 757648). KL was also supported by a Natural Environmental Research Council (NERC) UK Independent Research fellowship (NE/L011522/1). Figures 2, 3, 5 & 6 were finalized or produced with BioRender.com.

Author notes

K.L., M.K. and N.P. designed the study. N.P. carried out the DNA extractions, and conducted the genome analyses with input from K.L. and D.R.L. M.K. supervised the laboratory work and funded the study. N.P. and K.L. drafted the manuscript and all the authors helped in finalizing it.

Data availability

Raw reads of PacBio and Illumina samples as well as genome assemblies generated from the raw reads have been deposited on SRA (BioProject PRJNA939085). The accession numbers for the PacBio raw reads are SAMN33476292, SAMN33476293, SAMN33476294, SAMN33476295. The accession numbers for the Illumina raw reads are SAMN33454909, SAMN33454910, SAMN33454911, SAMN33454912, SAMN33454913, SAMN33454914, SAMN33454915, SAMN33454916, SAMN33454917, SAMN33454918, SAMN33454919, SAMN33454920, SAMN33454921, SAMN33454922, SAMN33454923, SAMN33454924, SAMN33454925, SAMN33454926, SAMN33454927, SAMN33454928, SAMN33454929. The non-chromosome-level and chromosome-level genome assemblies will be deposited in GenBank at the time of publication. Unix and R commands and Jupyter Notebooks used in the study will be made publicly available in GitHub at the time of publication.

741 References

742 Alonge M, Soyk S, Ramakrishnan S, Wang X, Goodwin S, Sedlazeck FJ, Lippman ZB, Schatz MC. 2019. RaGOO: Fast
743 and accurate reference-guided scaffolding of draft genomes. *Genome Biol.* 20.
744 Andrews S. 2010. FastQC: A quality control tool for high throughput sequence data. Available from:
745 http://www.bioinformatics.babraham.ac.uk/projects/fastqc/
746 Bao W, Kojima KK, Kohany O. 2015. Repbase Update, a database of repetitive elements in eukaryotic genomes.
747 *Mob. DNA* 6:4–9.
748 Barb JG, Bowers JE, Renaut S, Rey JI, Knapp SJ, Rieseberg LH, Burke JM. 2014. Chromosomal evolution and
749 patterns of introgression in *Helianthus*. *Genetics* 197:969–979.
750 Barnett DW, Garrison EK, Quinlan AR, Stŕmberg MP, Marth GT. 2011. Bamtools: A C++ API and toolkit for
751 analyzing and managing BAM files. *Bioinformatics* 27:1691–1692.
752 Basset P, Yannic G, Brünner H, Hausser J. 2006. Restricted gene flow at specific parts of the shrew genome in
753 chromosomal hybrid zones. *Evolution (N. Y).* 60:1718–1730.
754 Buchfink B, Xie C, Huson DH. 2014. Fast and sensitive protein alignment using DIAMOND. *Nat. Methods* 12:59–
755 60.
756 Butlin RK. 2005. Recombination and speciation. *Mol. Ecol.* 14:2621–2635.
757 Camacho C, Coulouris G, Avagyan V, Ma N, Papadopoulos J, Bealer K, Madden TL. 2009. BLAST+: Architecture
758 and applications. *BMC Bioinformatics* 10.
759 Chakraborty M, Baldwin-Brown JG, Long AD, Emerson JJ. 2016. Contiguous and accurate de novo assembly of
760 metazoan genomes with modest long read coverage. *Nucleic Acids Res.* 44.
761 Chang CC, Chow CC, Tellier LCAM, Vattikuti S, Purcell SM, Lee JJ. 2015. Second-generation PLINK: Rising to the
762 challenge of larger and richer datasets. *Gigascience* 4.
763 Charlesworth B, Campos JL, Jackson BC. 2018. Faster-X evolution: theory and evidence from *Drosophila*. *Mol.*
764 *Ecol.* 27:3753–3771.
765 Charlesworth B, Coyne JA, Barton NH. 1987. The relative rates of evolution of sex chromosomes and autosomes.
766 *Am. Nat.* 130:113–146.
767 Chen S, Zhou Y, Chen Y, Gu J. 2018. Fastp: An ultra-fast all-in-one FASTQ preprocessor. *Bioinformatics* 34:i884–
768 i890.
769 Connallon T, Olito C, Dutoit L, Papoli H, Ruzicka F, Yong L. 2018. Local adaptation and the evolution of inversions
770 on sex chromosomes and autosomes. *Philos. Trans. R. Soc. B Biol. Sci.* 373:20170423.
771 Counterman BA, Noor MAF. 2006. Multilocus test for introgression between the cactophilic species *Drosophila*
772 *mojavensis* and *Drosophila arizonae*. *Am. Nat.* 168:682–696.
773 Cruickshank TE, Hahn MW. 2014. Reanalysis suggests that genomic islands of speciation are due to reduced
774 diversity, not reduced gene flow. *Mol. Ecol.* 23:3133–3157.
775 Dagilis AJ, Kirkpatrick M. 2016. Prezygotic isolation, mating preferences, and the evolution of chromosomal
776 inversions. *Evolution* 70:1465–1472.
777 Dobin A, Davis CA, Schlesinger F, Drenkow J, Zaleski C, Jha S, Batut P, Chaisson M, Gingeras TR. 2013. STAR:
778 Ultrafast universal RNA-seq aligner. *Bioinformatics* 29:15–21.

Fang Z, Pyhäjärvi T, Weber AL, Dawe RK, Glaubitz JC, Sánchez González J de J, Ross-Ibarra C, Doebley J, Morrell PL, Ross-Ibarra J. 2012. Megabase-scale inversion polymorphism in the wild ancestor of maize. *Genetics* 191:883–894.

Faria R, Johannesson K, Butlin RK, Westram AM. 2018. Evolving Inversions. *Trends Ecol. Evol.* [Internet]:1–10. Available from: https://doi.org/10.1016/j.tree.2018.12.005

Faria R, Navarro A. 2010. Chromosomal speciation revisited: Rearranging theory with pieces of evidence. *Trends Ecol. Evol.* 25:660–669.

Fick SE, Hijmans RJ. 2017. WorldClim 2: new 1-km spatial resolution climate surfaces for global land areas. *Int. J. Climatol.* 37:4302–4315.

Fishman L, Stathos A, Beardsley PM, Williams CF, Hill JP. 2013. Chromosomal rearrangements and the genetics of reproductive barriers in *Mimulus* (monkey flowers). *Evolution (N. Y).* 67:2547–2560.

Flynn JM, Hubley R, Goubert C, Rosen J, Clark AG, Feschotte C, Smit AF. 2019. RepeatModeler2: Automated genomic discovery of transposable element families. *bioRxiv*.

Fuller ZL, Koury SA, Phadnis N, Schaeffer SW. 2019. How chromosomal rearrangements shape adaptation and speciation: Case studies in *Drosophila pseudoobscura* and its sibling species *Drosophila persimilis*. *Mol. Ecol.* 28:1283–1301.

Fuller ZL, Leonard CJ, Young RE, Schaeffer SW, Phadnis N. 2018. Ancestral polymorphisms explain the role of chromosomal inversions in speciation. *PLoS Genet.* 14.

Garrison E, Marth G. 2012. Haplotype-based variant detection from short-read sequencing. Available from: http://arxiv.org/abs/1207.3907

Gower G, Ragsdale AP, Bisschop G, Gutenkunst RN, Hartfield M, Noskova E, Schiffels S, Struck TJ, Kelleher J, Thornton KR. 2022. Demes: A standard format for demographic models. *Genetics* 222:iyac131.

Gremme G. 2013. Computational gene structure prediction.

Guan D, Guan D, McCarthy SA, Wood J, Howe K, Wang Y, Durbin R, Durbin R. 2020. Identifying and removing haplotypic duplication in primary genome assemblies. *Bioinformatics* 36:2896–2898.

Guerrero RF, Hahn MW. 2017. Speciation as a sieve for ancestral polymorphism. *Mol. Ecol.* 26:5362–5368.

Guerrero RF, Rousset F, Kirkpatrick M. 2012. Coalescent patterns for chromosomal inversions in divergent populations. *Philos. Trans. R. Soc. B Biol. Sci.* 367:430–438.

Halligan DL, Keightley PD. 2006. Ubiquitous selective constraints in the *Drosophila* genome revealed by a genome-wide interspecies comparison. *Genome Res.* 16:875–884.

Harrison RG, Larson EL. 2014. Hybridization, introgression, and the nature of species boundaries. *J. Hered.* 105:795–809.

Hijmans RJ, Etten J Van. 2020. raster: Geographic data analysis and modeling. R package version 2.8-19.

Hoff KJ, Lange S, Lomsadze A, Borodovsky M, Stanke M. 2016. BRAKER1: Unsupervised RNA-Seq-based genome annotation with GeneMark-ET and AUGUSTUS. *Bioinformatics* 32:767–769.

Hoff KJ, Lomsadze A, Borodovsky M, Stanke M. 2019. Whole-genome annotation with BRAKER. *Methods Mol. Biol.* 1962:65–95.

Hoffmann AA, Rieseberg L H. 2008. Revisiting the impact of inversions in evolution: From population genetic

817 markers to drivers of adaptive shifts and speciation? *Annu. Rev. Ecol. Evol. Syst.* 39:21–42.
818 Hoffmann AA, Rieseberg Loren H. 2008. The of impact revisiting in evolution: Inversions from genetic population
819 markers to drivers of adaptive shifts and speciation? *Annu. Rev. Ecol. Evol. Syst.* 39:21–42.
820 Hoikkala A, Poikela N. 2022. Adaptation and ecological speciation in seasonally varying environments at high
821 latitudes: *Drosophila virilis* group. *Fly (Austin).* [Internet] 16:85–104. Available from:
822 https://doi.org/10.1080/19336934.2021.2016327
823 Hopkins DP, Tyukmaeva VI, Gompert Z, Feder J, Nosil P. 2020. Functional genomics offers new tests of speciation
824 hypotheses. *Trends Ecol. Evol.* 35:968–971.
825 Hubley R, Finn RD, Clements J, Eddy SR, Jones TA, Bao W, Smit AFA, Wheeler TJ. 2016. The Dfam database of
826 repetitive DNA families. *Nucleic Acids Res.* 44:D81–D89.
827 Jackson BC. 2011. Recombination-suppression: How many mechanisms for chromosomal speciation? *Genetica*
828 139:393–402.
829 Jeffares DC, Jolly C, Hoti M, Speed D, Shaw L, Rallis C, Balloux F, Dessimoz C, Bähler J, Sedlazeck FJ. 2017.
830 Transient structural variations have strong effects on quantitative traits and reproductive isolation in
831 fission yeast. *Nat. Commun.* 8.
832 Kapun M, Flatt T. 2019. The adaptive significance of chromosomal inversion polymorphisms in *Drosophila*
833 *melanogaster*. *Mol. Ecol.* 28:1263–1282.
834 Kapun M, Schmidt C, Durmaz E, Schmidt PS, Flatt T. 2016. Parallel effects of the inversion In(3R)Payne on body
835 size across the North American and Australian clines in *Drosophila melanogaster*. *J. Evol. Biol.* 29:1059–
836 1072.
837 Keightley PD, Ness RW, Halligan DL, Haddrill PR. 2014. Estimation of the spontaneous mutation rate per
838 nucleotide site in a *Drosophila melanogaster* full-sib family. *Genetics* 196:313–320.
839 Kirkpatrick M, Barton N. 2006. Chromosome inversions, local adaptation and speciation. *Genetics* 173:419–434.
840 Korunes KL, Noor MAF. 2018. Pervasive gene conversion in chromosomal inversion heterozygotes. *Mol. Ecol.*:1–
841 14.
842 Kulathinal RJ, Stevison LS, Noor MAF. 2009. The genomics of speciation in *Drosophila*: Diversity, divergence, and
843 introgression estimated using low-coverage genome sequencing. *PLoS Genet.* 5.
844 Laetsch DR, Bisschop G, Martin SH, Aeschbacher S, Lohse K. 2022. Demographically explicit scans for barriers to
845 gene flow using gIMble. *bioRxiv*.
846 Laetsch DR, Blaxter ML. 2017. BlobTools: Interrogation of genome assemblies. *F1000Research 2017* 6:1–16.
847 Lê S, Josse J, Husson F. 2008. FactoMineR: An R Package for multivariate analysis. *J. Stat. Softw.* 25:1–18.
848 Li H. 2018. Minimap2: Pairwise alignment for nucleotide sequences. *Bioinformatics* 34:3094–3100.
849 Li H, Durbin R. 2009. Fast and accurate short read alignment with Burrows – Wheeler transform. *Bioinformatics*
850 25:1754–1760.
851 Li H, Handsaker B, Wysoker A, Fennell T, Ruan J, Homer N, Marth G, Abecasis G, Durbin R, 1000 Genome Project
852 Data Processing Subgroup. 2009. The Sequence Alignment/Map (SAM) Format and SAMtools.
853 *Bioinformatics* [Internet] 25:2078–2079. Available from: http://samtools.sourceforge.net
854 Lohse K, Clarke M, Ritchie MG, Etges WJ. 2015. Genome-wide tests for introgression between cactophilic

855 *Drosophila* implicate a role of inversions during speciation. *Evolution (N. Y).* 69:1178–1190.
856 Lomsadze A, Burns PD, Borodovsky M. 2014. Integration of mapped RNA-Seq reads into automatic training of
857 eukaryotic gene finding algorithm. *Nucleic Acids Res.* 42.
858 Lowry DB, Willis JH. 2010. A widespread chromosomal inversion polymorphism contributes to a major life-
859 history transition, local adaptation, and reproductive isolation. *PLoS Biol.* 8.
860 Lundberg M, Mackintosh A, Petri A, Bensch S. 2023. Inversions maintain differences between migratory
861 phenotypes of a songbird. *Nat. Commun.* 14:452.
862 Matzkin LM, Merritt TJS, Zhu CT, Eanes WF. 2005. The structure and population genetics of the breakpoints
863 associated with the cosmopolitan chromosomal inversion In(3R)Payne in *Drosophila melanogaster*.
864 *Genetics* 170:1143–1152.
865 Michel AP, Grushko O, Guelbeogo WM, Lobo NF, Sagnon N, Costantini C, Besansky NJ. 2006. Divergence with
866 gene flow in *Anopheles funestus* from the Sudan Savanna of Burkina Faso, West Africa. *Genetics* 173:1389–
867 1395.
868 Miller DE, Staber C, Zeitlinger J, Hawley RS. 2018. Highly contiguous genome assemblies of 15 *Drosophila* species
869 generated using nanopore sequencing. *G3 Genes, Genomes, Genet.* 8:3131–3141.
870 Navarro A, Barton NH. 2003. Accumulating postzygotic isolation genes in parapatry: A new twist on
871 chromosomal speciation. *Evolution (N. Y).* 57:447–459.
872 Noor MAF, Bennett SM. 2009. Islands of speciation or mirages in the desert? Examining the role of restricted
873 recombination in maintaining species. *Heredity (Edinb).* 103:439–444.
874 Noor MAF, Garfield DA, Schaeffer SW, Machado CA. 2007. Divergence between the *Drosophila pseudoobscura*
875 and *D. persimilis* genome sequences in relation to chromosomal inversions. *Genetics* 177:1417–1428.
876 Noor MAF, Grams KL, Bertucci LA, Reiland J. 2001. Chromosomal inversions and the reproductive isolation of
877 species. *Proc. Natl. Acad. Sci. U. S. A.* 98:12084–12088.
878 Parker DJ, Envall T, Ritchie MG, Kankare M. 2021. Sex-specific responses to cold in a very cold-tolerant, northern
879 *Drosophila* species. *Heredity (Edinb).* [Internet] 126:695–705. Available from:
880 http://dx.doi.org/10.1038/s41437-020-00398-2
881 Parker DJ, Wiberg RAW, Trivedi U, Tyukmaeva VI, Gharbi K, Butlin RK, Hoikkala A, Kankare M, Ritchie MG. 2018.
882 Inter and intraspecific genomic divergence in *Drosophila montana* shows evidence for cold adaptation.
883 *Genome Biol. Evol.* 10:2086–2101.
884 Patterson JT. 1952. Revision of the *montana* complex of the *virilis* species group. *Univerisity Texas Publ.*
885 5204:20–34.
886 Poikela N, Kinnunen J, Wurdack M, Kauranen H, Schmitt T, Kankare M, Snook RR, Hoikkala A. 2019. Strength of
887 sexual and postmating prezygotic barriers varies between sympatric populations with different histories
888 and species abundances. *Evolution* 73:1182–1199.
889 Poikela N, Laetsch DR, Kankare M, Hoikkala A, Lohse K. 2022. Experimental introgression in *Drosophila*:
890 asymmetric postzygotic isolation associated with chromosomal inversions and an incompatibility locus on
891 the X chromosome. *Mol. Ecol.* 00:1–13.
892 Poikela N, Tyukmaeva V, Hoikkala A, Kankare M. 2021. Multiple paths to cold tolerance: The role of

environmental cues, morphological traits and the circadian clock gene *vrille*. *BMC Ecol. Evol.* [Internet] 21:1–20. Available from: https://doi.org/10.1186/s12862-021-01849-y

Rausch T, Zichner T, Schlattl A, Stütz AM, Benes V, Korbel JO. 2012. DELLY: Structural variant discovery by integrated paired-end and split-read analysis. *Bioinformatics* 28.

Ruan J, Li H. 2020. Fast and accurate long-read assembly with wtdbg2. *Nat. Methods* 17:155–158.

Schäfer MA, Mazzi D, Klappert K, Kauranen H, Vieira J, Hoikkala A, Ritchie MG, Schlötterer C. 2010. A microsatellite linkage map for *Drosophila montana* shows large variation in recombination rates, and a courtship song trait maps to an area of low recombination. *J. Evol. Biol.* 23:518–527.

Sedlazeck FJ, Rescheneder P, Smolka M, Fang H, Nattestad M, Von Haeseler A, Schatz MC. 2018. Accurate detection of complex structural variations using single-molecule sequencing. *Nat. Methods* 15:461–468.

Seehausen O, Butlin RK, Keller I, Wagner CE, Boughman JW, Hohenlohe PA, Peichel CL, Saetre GP, Bank C, Brännström Å, et al. 2014. Genomics and the origin of species. *Nat. Rev. Genet.* 15:176–192.

Seppey M, Manni M, Zdobnow EM. 2019. BUSCO: Assessing genome assembly and annotation completeness. *Gene Predict. methods Protoc.*:227–245.

Servedio MR, Noor MAF. 2003. The role of reinforcement in speciation: Theory and data. *Source Annu. Rev. Ecol. Evol. Syst.* [Internet] 34:339–364. Available from: https://about.jstor.org/terms

Smit A, Hubley R, Green P. 2015. RepeatMasker Open-4.0.

Stanke M, Diekhans M, Baertsch R, Haussler D. 2008. Using native and syntenically mapped cDNA alignments to improve de novo gene finding. *Bioinformatics* 24:637–644.

Stanke M, Schöffmann O, Morgenstern B, Waack S. 2006. Gene prediction in eukaryotes with a generalized hidden Markov model that uses hints from external sources. *BMC Bioinformatics* 7.

Stone WS, Guest WC, Wilson FD. 1960. The evolutionary implications of the cytological polymorphism and phylogeny of the *virilis* group of *Drosophila*. *Proc. Natl. Acad. Sci.* 46:350–361.

Sturtevant AH. 1921. A case of rearrangement of genes in *Drosophila*. *Proc. Natl. Acad. Sci. U. S. A.* 7:235–237.

Tarasov A, Vilella AJ, Cuppen E, Nijman IJ, Prins P. 2015. Sambamba: Fast processing of NGS alignment formats. *Bioi* 31:2032–2034.

Thorvaldsdóttir H, Robinson JT, Mesirov JP. 2013. Integrative Genomics Viewer (IGV): high-performance genomics data visualization and exploration. *Brief. Bioinform.* 14:178–192.

Throckmorton LH. 1982. The *virilis* species group. *Genet. Bioogy Drosoph.* 3:227–296.

Trickett AJ, Butlin RK. 1994. Recombination suppressors and the evolution of new species. *Heredity (Edinb).* 73:339–345.

Tyukmaeva VI, Lankinen P, Kinnunen J, Kauranen H, Hoikkala A. 2020. Latitudinal clines in the timing and temperature-sensitivity of photoperiodic reproductive diapause in *Drosophila montana*. *Ecography (Cop.).* 43:1–10.

Vicoso B, Charlesworth B. 2006. Evolution on the X chromosome: Unusual patterns and processes. *Nat. Rev. Genet.* 7:645–653.

Walker BJ, Abeel T, Shea T, Priest M, Abouelliel A, Sakthikumar S, Cuomo CA, Zeng Q, Wortman J, Young SK, et al. 2014. Pilon: An integrated tool for comprehensive microbial variant detection and genome assembly

931 improvement. *PLoS One* 9.
932 Wall JD. 2003. Estimating ancestral population sizes and divergence times. *Genetics* 163:395–404.
933 Wallberg A, Schöning C, Webster MT, Hasselmann M. 2017. Two extended haplotype blocks are associated with
934 adaptation to high altitude habitats in East African honey bees. *PLoS Genet.* 13.
935 Wellenreuther M, Bernatchez L. 2018. Eco-evolutionary genomics of chromosomal inversions. *Trends Ecol. Evol.*
936 33:427–440.
937 White NJ, Snook RR, Eyres I. 2020. The past and future of experimental speciation. *Trends Ecol. Evol.* 35:10–21.
938 Yang H, Jaime M, Polihronakis M, Kanegawa K, Markow T, Kaneshiro K, Oliver B. 2018. Re-annotation of eight
939 *Drosophila* genomes. *Life Sci. Alliance* 1.
940 Yusuf L, Tyukmaeave V, Hoikkala A, Ritchie M. 2022. Divergence and introgression among the *virilis* group of
941 *Drosophila*. *bioRxiv*:https://doi.org/10.1101/2022.01.11.475832.
942 Zimin A V., Puiu D, Luo MC, Zhu T, Koren S, Marçais G, Yorke JA, Dvořák J, Salzberg SL. 2017. Hybrid assembly of
943 the large and highly repetitive genome of *Aegilops tauschii*, a progenitor of bread wheat, with the
944 MaSuRCA mega-reads algorithm. *Genome Res.* 27:787–792.